polymers

MDPI

Article

Butyl Rubber Nanocomposites with Monolayer MoS_2 Additives: Structural Characteristics, Enhanced Mechanical, and Gas Barrier Properties

Chi-Yang Tsai [1], Shuian-Yin Lin [2] and Hsieh-Chih Tsai [1,*]

[1] Graduate Institute of Applied Science and Technology, National Taiwan University of Science and Technology, Taipei 10607, Taiwan; charlie810903@gmail.com

[2] Industrial Technology Research Institute, Biomedical Technology and Device Research Laboratories, Hsinchu 31057, Taiwan; sylin@biip-mdcc.org

* Correspondence: h.c.tsai@mail.ntust.edu.tw; Tel.: +886-2-2730-3779; Fax: +886-2-2730-3733

Received: 31 January 2018; Accepted: 24 February 2018; Published: 27 February 2018

Abstract: Emerging two-dimensional (2D) materialsm, such as molybdenum disulfide (MoS_2), offer opportunities to tailor the mechanical and gas barrier properties of polymeric materials. In this study, MoS_2 was exfoliated to monolayers by modification with ethanethiol and nonanethiol. The thicknesses of resulting MoS_2 monolayers were 0.7 nm for MoS_2-ethanethiol and 1.1 nm for MoS_2-nonanethiol. MoS_2 monolayers were added to chlorobutyl rubber to prepare MoS_2-butyl rubber nanocomposites at concentrations of 0.5, 1, 3, and 5 phr. The tensile stress showed a maximum enhancement of about 30.7% for MoS_2-ethanethiol-butyl rubber and 34.8% for MoS_2-nonanethiol-butyl rubber when compared to pure chlorobutyl rubber. In addition, the gas barrier properties were increased by 53.5% in MoS_2-ethanethiol-butyl rubber and 49.6% in MoS_2-nonanethiol-butyl rubber. MoS_2 nanosheets thus enhanced the mechanical and gas barrier properties of chlorobutyl rubber. The nanocomposites that are presented here may be used to manufacture pharmaceutical stoppers with high mechanical and gas barrier properties.

Keywords: layered structures; polymer-matrix composites; mechanical properties; gas barrier properties

1. Introduction

Since the discovery of graphene, two-dimensional inorganic materials, such as MoS_2, have attracted great attention. MoS_2 has a structure similar to that of graphite; two layers of sulfur and one layer of molybdenum atoms in a sandwiched structure make up its hexagonal crystal lattice structure. MoS_2 is unreactive, unaffected by both acids and oxygen, and has a low coefficient of friction due to weak van der Waals interactions between the layers. As such, it is widely used as a dry lubricant. In addition, MoS_2 can be exfoliated into nanolayers without the need for complex methods. MoS_2 nanosheets have previously been utilized in transistors [1], biomaterials [2], and nanocomposites [3], and can also be added to polymers as a filler material; because of the high band gap of MoS_2, the electronic properties of the polymer matrices are not changed. A common reason to add fillers to polymers is to improve their mechanical properties. For example, polymer chains can interact with the nanosheet surfaces, resulting in reinforcements in all directions from the nanosheets. For the latter, it is important to fully exfoliate the two-dimensional inorganic materials to increase the surface area [4].

Many studies have reported the use of nanoscale fillers such as clay, reduced graphene oxide, and MoS_2 to improve the mechanical and gas barrier properties of polymer materials for a variety of applications. For example, the optimal mechanical or barrier properties were observed for exfoliated or intercalated polymer/clay nanocomposites, but using a high clay content of 5–10 wt % [5–7]. Clay

is difficult to exfoliate due to the many cations in the spacing between the layers of the material. In addition, clay is hydrophilic and cannot disperse well in hydrophobic polymers. However, quaternary ammonium cation salt can usually act as modifiers to enable exfoliation and dispersion of clay molecules in polymer matrices [8]. Graphene consists of two-dimensional sheets of sp^2-bonded carbon with a high specific surface area. Graphene-based nanocomposites play an important role because of their favorable mechanical, electrical, and barrier properties. Their barrier properties, for example, are much better than those of clay nanofillers [9–11]. Some applications require improvements in the mechanical properties and thermal stability of a polymer matrix, while maintaining the polymer's electrical insulation properties. Graphene, as a highly conductive material, does not appear to be a good filler material choice for such applications. In addition, fillers have to be uniformly dispersed in a polymer matrix. However, exfoliation of graphene is still unpractical, with the most common method involving the treatment of graphite with strong oxidizers to obtain exfoliated graphene oxide. MoS_2 exfoliation into nanosheets, on the other hand, can be achieved in a one-step, simple method at low MoS_2 loading rates, and is thus more economical. MoS_2 nanosheets are therefore an excellent alternative to clay and graphene-based materials for enhancing the properties of polymer matrices. MoS_2 has been reported as filler to manufacture photo-mechanical response material [12], gas selective membranes [13], and supercapacitor [14].

Due to weak van der Waals interactions between the layers of bulk MoS_2, MoS_2 nanosheets can easily be prepared by ultrasonication. A common method for the exfoliation of MoS_2 involves the use of lithium ions to intercalate the MoS_2 nanosheets. However, it is hard to disperse MoS_2 nanosheets in nonpolar polymers without modifying their surfaces with organic ligands. In previous works, ultrasonicating bulk MoS_2 powder produced a number of sulfur vacancies on the surface of a MoS_2 nanosheet, which were reported to act as targets for surface modification [15,16]. Here, thiol compounds were selected as modifiers of MoS_2 nanosheets to increase the affinity between the nanosheets and polymer matrix. With a greater degree of MoS_2 nanosheet dispersion, a greater degree of reinforcement would be expected in the nanocomposite.

Chlorobutyl rubber is often used in tires, gas masks, and chemical agent packaging because of its good mechanical and gas barrier properties. Unlike conventional butyl rubber, with a lack of double bond on the backbone of polymer chain, the vulcanization of chorobutyl rubber is more efficiently. The aim of this study was to enhance the mechanical and gas barrier properties of chemical agent packaging materials, which require enhanced gas barrier properties for the storage of chemical agents. For this reason, chlorobutyl rubber with added MoS_2 was studied as a suitable material. Exfoliated MoS_2 nanosheets surface-modified by ethanethiol and nonanethiol to enhance their affinity to polymers were expected to disperse well in chlorobutyl rubber and result in improved mechanical and gas barrier properties. Herein, the effects of ethanethiol- and nonanethiol-modified MoS_2 nanosheets are compared for various MoS_2 concentrations.

2. Materials and Methods

2.1. Materials

Chlorobutyl rubber (Mooney viscosity [ML_{1+8} 100 °C]: ~41–49) was obtain from ExxonMobil Chemical (Houston, TX, USA); MoS_2 from Alfa Aesar (Haverhill, MA, USA); hexane from Fisher Chemical (Hampton, NH, USA); ethanethiol from Sigma-Aldrich (St. Louis, MO, USA); nonanethiol from Acros (Hampton, NH, USA); ethylenethiourea(2-mercaptoimidazoline) from Kawaguchi Chemical Industry (Kawaguchi, Japan); and silicon dioxide (TOKUSIL 255, with surface area BET 177 m^2/g) was obtained from OSC Group (Miaoli, Taiwan).

2.2. Exfoliation of MoS_2

For the exfoliation of MoS_2, 400 mg MoS_2 powder and 20 mL hexane were mixed in 20-mL vials and ethanethiol and nonanethiol were added to each vial. Ultrasonication to exfoliate MoS_2 was

applied in a bath for 24 h. After ultrasonication, the contents of the vials were allowed to settle, and exfoliated MoS_2 was obtained as the suspension.

2.3. Preparation of MoS_2-butyl Rubber Nanocomposites

MoS_2-butyl rubber nanocomposites were prepared with various MoS_2 concentrations 0.5, 1, 3, and 5 parts per hundreds of rubber (phr). The previously obtained MoS_2 nanosheets were mixed with chlorobutyl rubber and were dissolved in hexane under mechanical stirring for 1 h to achieve a homogenous mixture. The hexane was then evaporated and the samples thus obtained were dried at 100 °C in a vacuum oven for 12 h to completely remove the solvent. The samples were compounded by two-roll-mill with 20 phr silicon dioxide as a widely used filler for rubber to improve the wear resistance and also acts as a reinforcing agent and using 0.5 phr ethylenethiourea(2-mercaptoimidazoline) as the curing reagent. After compression molding at 185 °C at a pressure of 50 kgf/cm^2 for 10 min, MoS_2-butyl rubber nanocomposite samples with dimensions of 15 cm × 15 cm and a 1-mm thickness were obtained.

2.4. Characterization

The morphologies of the MoS_2 nanosheets modified by ethanethiol and nonanethiol were observed using a Tecnai™ G2 F-20 (Philips, Amsterdam, Netherlands) transmission electron microscope (TEM). Raman spectra and Raman maps were obtained using an NRS5100 (JASCO, Tokyo, Japan) spectrometer. Cross-sectional images were obtained using a JSM-6500F (JEOL, Tokyo, Japan) scanning electron microscope (SEM); and, composite samples were cooled in liquid nitrogen and cut by a scalpel to prepare the samples for backscattered electron (BSE) imaging. Atomic force microscopy (AFM) was performed using a NX10 system (Park, Suwon, Korea). X-ray diffraction (XRD) was performed using a D8 SSS (Bruker, Billerica, MA, USA). UV-Vis spectra were obtained using a V-730 spectrometer (JASCO, Tokyo, Japan). Dynamic mechanical analysis was performed using a Q800 (TA Instruments, New Castle, DE, USA), while stress-strain curves were measured using a TS-2000 with a crosshead speed of 500 mm/min. The oxygen transmission rates were measured according to the ASTM D3985 standard using the OX-TRAN 2/61 (Mocon Inc., Minneapolis, MN, USA) at 23 °C and a relative humidity of 0%; film specimens of 5 cm in diameter and 1 mm in thickness were fixed between two chambers, and oxygen filled the upper chamber while nitrogen filled the lower chamber.

3. Results and Discussion

3.1. Exfoliation of MoS_2

Scheme 1 outlines the overall procedure for the preparation of the MoS_2 nanosheets and the production of MoS_2-butyl rubber nanocomposites. The exfoliation of MoS_2 was achieved by bath ultrasonication of bulk MoS_2 powder in hexane. It has previously been reported that this exfoliation process can produce a number of structural defects, such as S vacancy defects [17,18]. Then, MoS_2 nanosheets can be modified with thiol ligands. Ethanethiol and nonanethiol were used as the surface modifiers in this study. The carbon chains of these two thiols were hypothesized to modify the surface of MoS_2 to enhance its compatibility with chlorobutyl rubber. The organic modification of the surface and robust nature of the modifiers ensured good dispersion and a dramatically enhanced properties of the polymer materials.

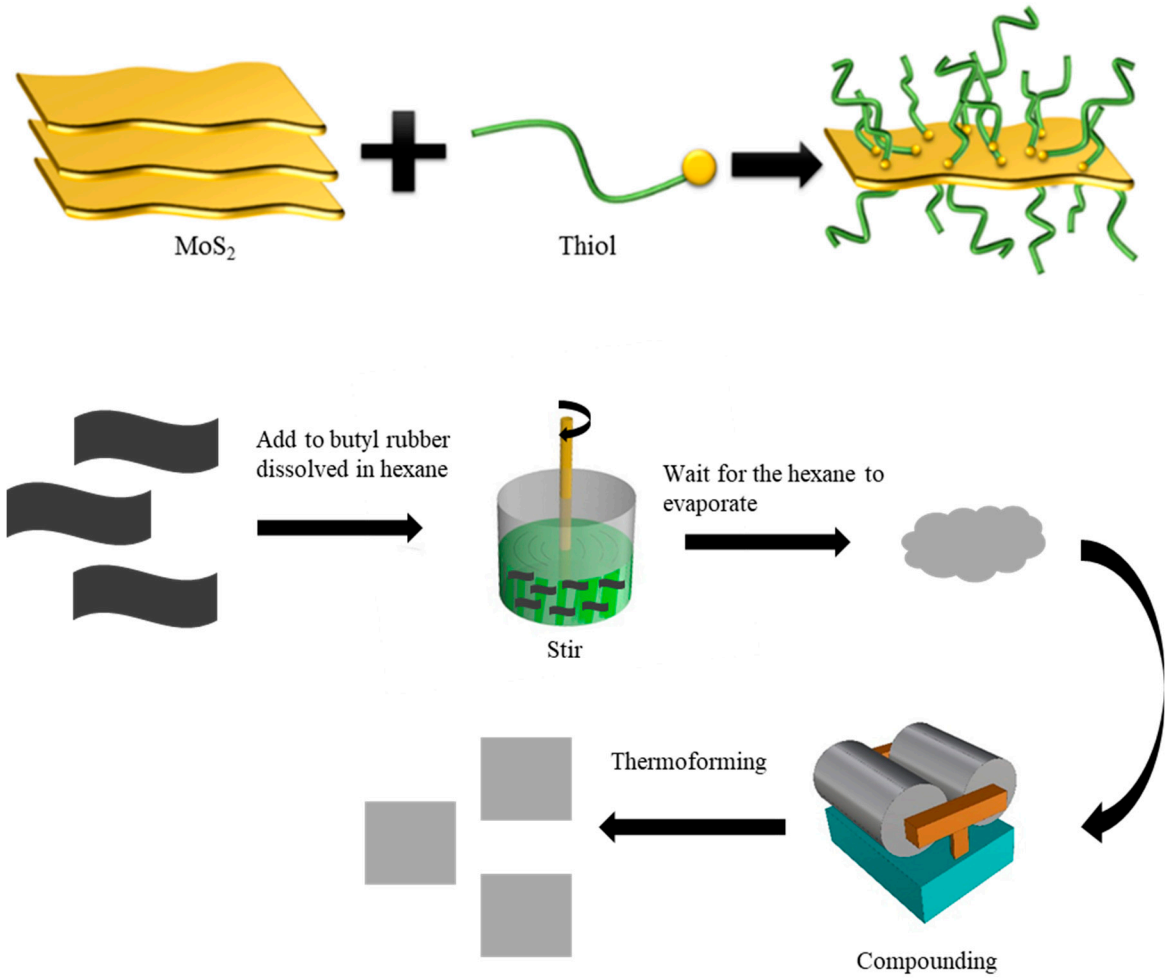

Scheme 1. Schematic illustration for exfoliation modification of MoS_2 and corresponding production of chlorobutyl rubber-based nanocomposites.

The morphologies of MoS_2 nanosheets modified by ethanethiol and nonanethiol are presented in TEM images (Figure 1a,b). The hexagonal structure of MoS_2 modified by ethanethiol and nonanethiol was clearly visible in high-resolution TEM images (Figure 1c,d). It can be inferred that these MoS_2 nanosheets were either several layers thick or monolayers, because the hexagonal lattice structure of MoS_2 was visible. The latter indicates that the crystal structures of MoS_2-ethanethiol and MoS_2-nonanethiol were retained during ultrasonication [19]. Raman spectra were used to confirm the modification of the MoS_2 nanosheet surfaces by ethanethiol and nonanethiol (Figure 2). Peaks were seen at ~380 cm^{-1} (E^1_{2g}, in-plane vibrations) and ~410 cm^{-1} (A_{1g}, out-of-plane vibrations), characteristic of the MoS_2 trigonal structure. Peaks at ~680 and ~1100 cm^{-1}, which indicate carbon-sulfur (ν_{cs}) [20] and carbon-carbon bonds (ν_{cc}) [21], respectively, were noted for the modified MoS_2. These results indicate that the surface of MoS_2 was successfully modified by ethanethiol and nonanethiol.

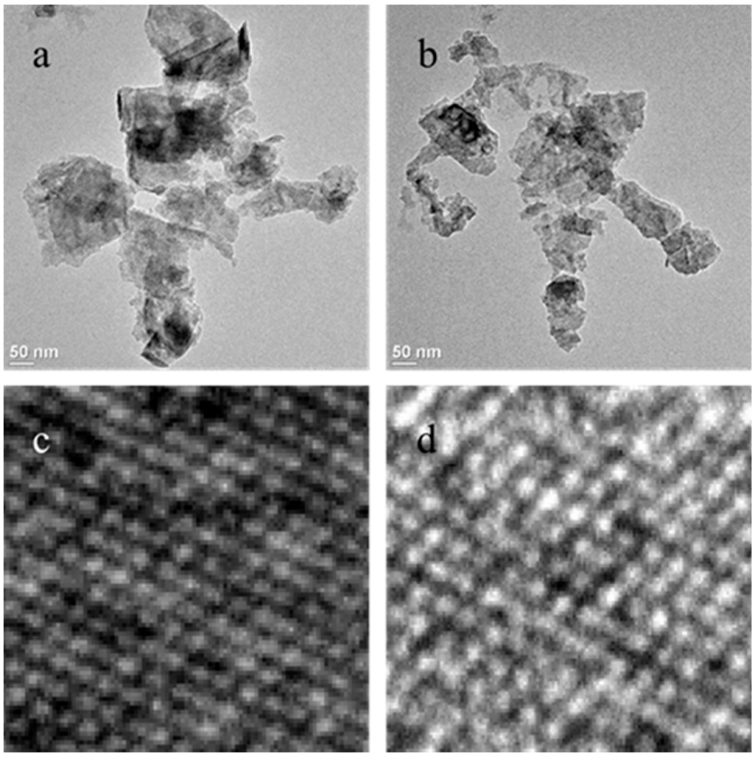

Figure 1. Transmission electron microscope (TEM) images of MoS_2 nanosheets. (**a**,**c**) Low- and high-resolution images of MoS_2-ethanethiol; (**b**,**d**) low- and high-resolution images of MoS_2-nonanethiol.

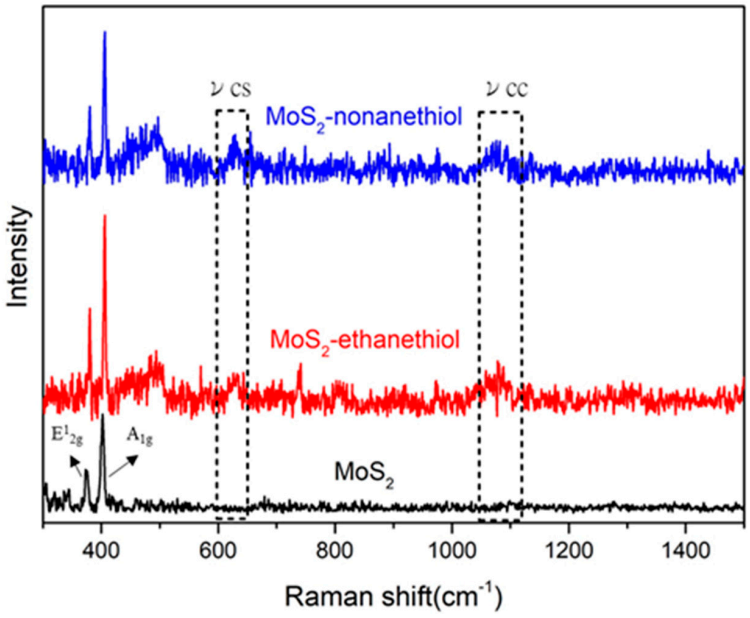

Figure 2. Raman spectra of MoS_2 and thiol-modified MoS_2.

The thicknesses of the exfoliated nanosheets were monitored through AFM examination of the exfoliated samples. The thickness of bulk MoS_2 was ~90–120 nm (Figure 3a), while that of MoS_2-ethanethiol was ~0.7 nm (Figure 3b) and that of MoS_2-nonanethiol was ~1.1 nm (Figure 3c), values that correspond to that of ~0.65 nm in previous reports on the thickness of MoS_2 monolayers [1]. The thicknesses obtained here being greater than the typical thickness of a single-layer MoS_2 sheet

may be attributed to thiol conjugation on the surface of MoS_2 [22]. Blue-shifts of UV-Vis spectra are dependent on changes in the band gap energy, which can be obtained from the wavelengths in UV-Vis spectra from the following equation:

$$\text{Band gap energy } (E) = (hc)/\lambda \quad (1)$$

where hc is Planck's constant and λ is the wavelength. Bulk MoS_2 is an indirect semiconductor with a band gap of ~1.2 eV, which increases to ~1.8 and ~1.9 eV for monolayers of MoS_2 [23,24]. To obtain the optimum parameters for exfoliation, the number of MoS_2 nanosheet layers was measured for various concentrations of ethanethiol and nonanethiol by UV-Vis spectra (Figure 4). The MoS_2-ethanethiol sample in Figure 4a shows a blue-shift from 697 to 688 nm. The latter wavelength of 688 nm corresponds to a band gap value of 1.80 eV. For MoS_2-nonanethiol in Figure 4b, a blue-shift from 697 to 685 nm can be observed. The latter wavelength of 685 nm corresponds to a band gap value of 1.81 eV. The conditions to exfoliate MoS_2 into monolayer involved the addition of 0.5 mL of either ethanethiol or nonanethiol with 400 mg bulk MoS_2 powder into 20 mL hexane. The exfoliation efficiency for MoS_2 that was treated with nonanethiol was greater than that of MoS_2 treated with ethanethiol.

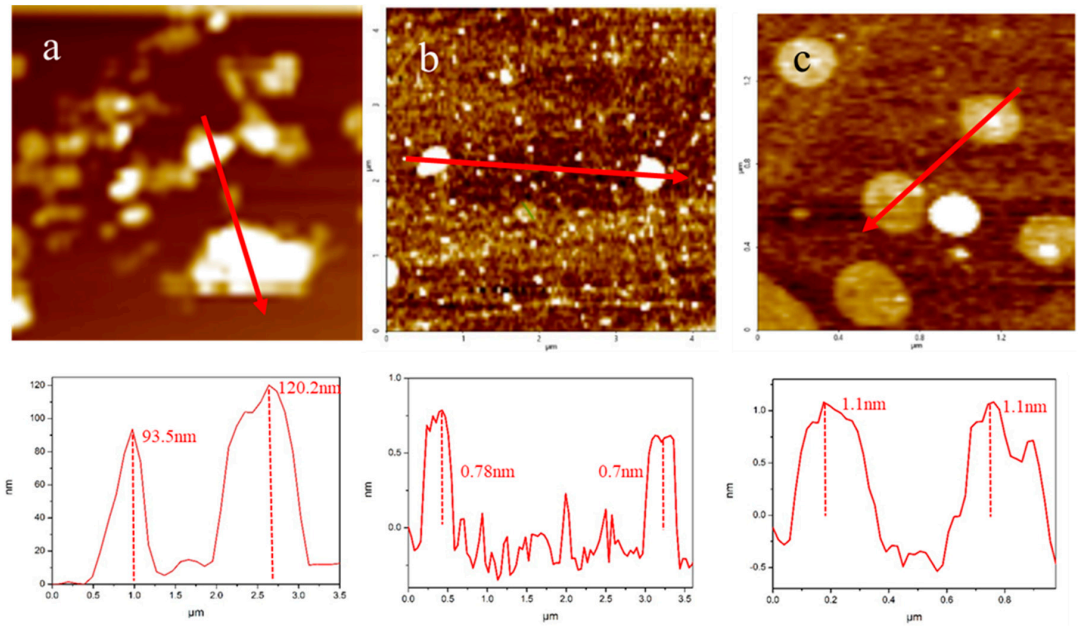

Figure 3. Atomic force microscope (AFM) images of: (**a**) bulk MoS_2, (**b**) MoS_2-ethanethiol, and (**c**) MoS_2-nonanethiol.

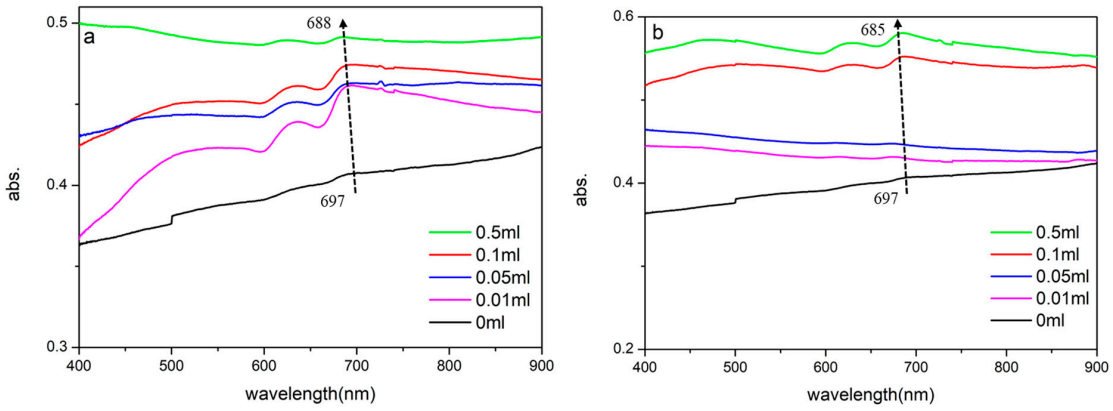

Figure 4. UV-Vis spectra: (**a**) MoS_2-ethanethiol and (**b**) MoS_2-nonanethiol.

3.2. Characterization of MoS_2-butyl rubber Nanocomposites

XRD was performed to characterize the obtained layered-structure materials and partially evaluate the dispersion state of layered nanofillers in the polymer composites. XRD scans of the polymer nanocomposites showed a nanofiller peak and a shift to a lower 2θ or larger d-spacing value when compared to bulk MoS_2. The peak shift indicates an expansion of the d-spacing of MoS_2 nanosheets; it was inferred that polymer chains had been intercalated in the MoS_2 nanosheets. For completely exfoliated layered nanofillers, no XRD peaks were expected for the nanocomposites, since they should not show regular spacing of the sheets [25].

The XRD patterns (Figure 5) of the MoS_2-butyl rubber nanocomposites confirm the intercalation of chlorobutyl rubber in the MoS_2 nanosheet interlayers by showing a decrease in 2θ value as the concentration of MoS_2 increased. The (002) peak of pure MoS_2 was at 2θ = 14.44°, corresponding to a d-spacing value of 0.3088 nm. After adding MoS_2 to chlorobutyl rubber, the 2θ peak of the (002) plane shifted to lower angles, associated with intercalation in nanocomposites. For MoS_2-ethanethiol-butyl rubber, the peak at 2θ = 14.44° (d = 0.3088 nm) for 0 phr shifted to 2θ = 14.40° (d = 0.3097 nm), and 2θ = 14.38° (d = 0.3102 nm) for the samples with 3 and 5 phr MoS_2, respectively. For MoS_2-nonanethiol-butyl rubber, the peak was at 2θ = 14.36° for the 0.5-phr sample, which indicates that the d-spacing of MoS_2 increased when MoS_2 nanosheets were inserted into the chlorobutyl rubber chains. The latter illustrates that, between the exfoliation and intercalation, the nanocomposites can be driven toward full exfoliation by decreasing the content of MoS_2 nanosheets. The greater shift at low concentrations indicates that nonanethiol is a more suitable modifier for MoS_2 exfoliation than ethanethiol.

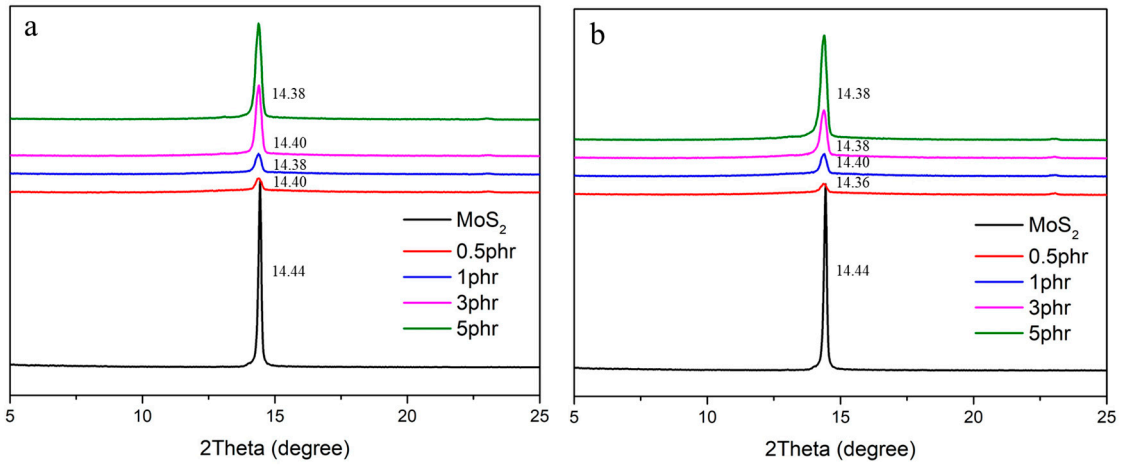

Figure 5. X-ray diffraction (XRD) patterns of MoS_2-butyl rubber nanocomposites: (**a**) MoS_2-ethanethiol-butyl rubber and (**b**) MoS_2-nonanethiol-butyl rubber.

The SEM-BSE images (Figure 6) of MoS_2-butyl rubber nanocomposite cross-sections demonstrate the dispersion of MoS_2 nanosheets in chlorobutyl rubber obtained at different concentrations. These micrographs confirm that, at higher concentrations, i.e., 3 and 5 phr, big clusters of agglomerated ethanethiol- and nonanethiol-modified MoS_2 were present. At lower concentrations, i.e., 0.5 and 1 phr, on the other hand, MoS_2 was homogeneously dispersed in chlorobutyl rubber.

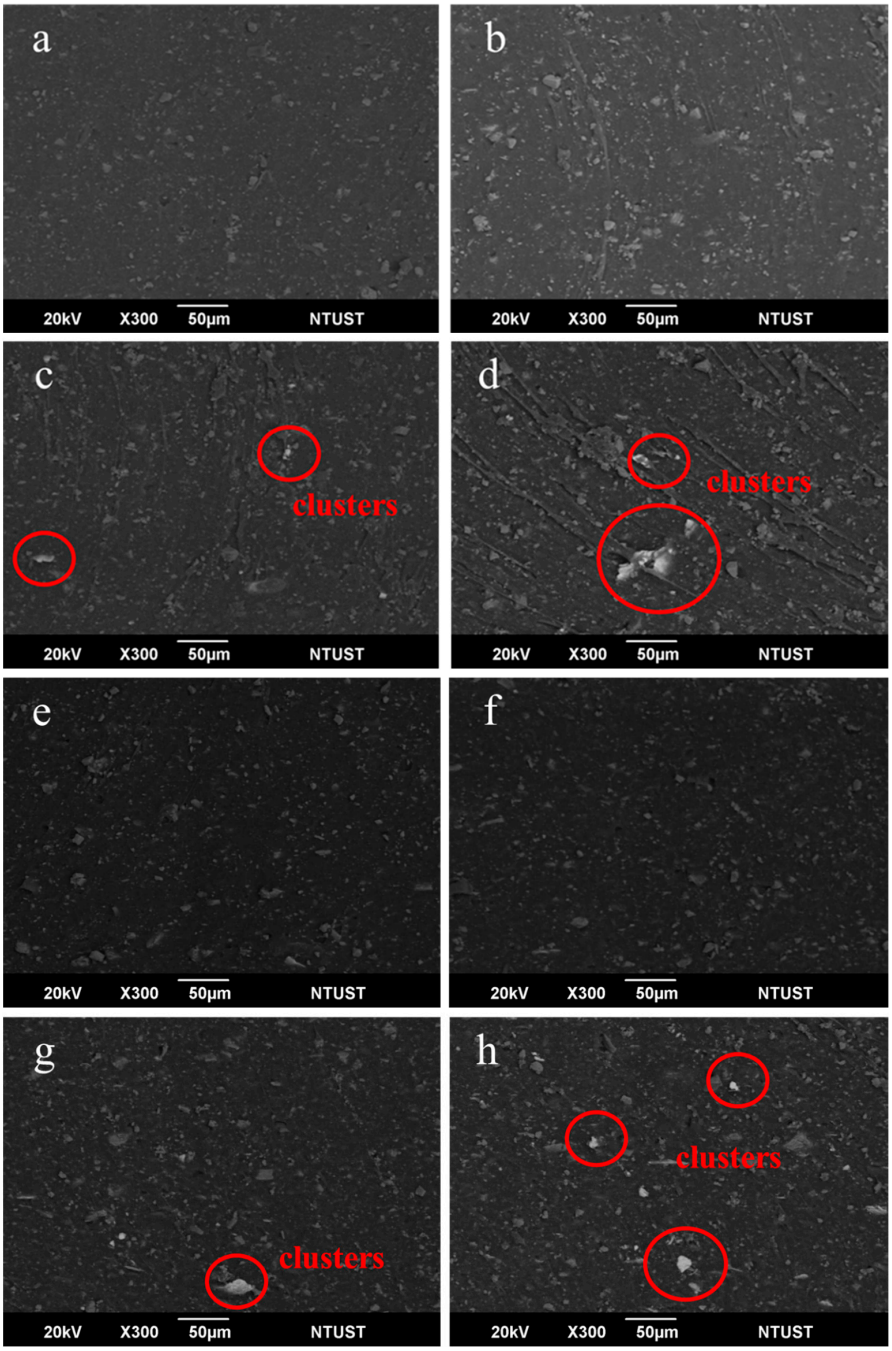

Figure 6. Scanning electron microscope backscattered electrons (SEM-BSE) cross-sectional images for MoS_2-butyl rubber with different concentrations of MoS_2 with either ethanethiol or nonanethiol: (**a**) 0.5 phr, ethanethiol; (**b**) 1 phr, ethanethiol; (**c**) 3 phr, ethanethiol; (**d**) 5 phr, ethanethiol; (**e**) 0.5 phr, nonanethiol; (**f**) 1 phr, nonanethiol; (**g**) 3 phr, nonanethiol; and, (**h**) 5 phr, nonanethiol.

The typical Raman peaks for MoS2-butyl rubber nanocomposites are shown in Figure 7. The peaks at ~380 and ~410 cm^{-1} correspond to MoS2, while the peaks at ~720, ~820, ~910, and ~1080 cm^{-1} correspond to chlorobutyl rubber. Raman mapping (Figure 8) was used to further confirm the dispersion state of MoS_2 nanosheets at different MoS_2 concentrations. Figure 8 shows the intensity maps of the A_{1g} peak (~410 cm^{-1}) of MoS_2 for nanocomposites with different concentrations of modified MoS_2 nanosheets. The Raman mapping images correspond well with the SEM-BSE images (Figure 6). At low concentrations of MoS_2 nanosheets, their distribution was uniform,

which implies homogeneous dispersion in chlorobutyl rubber. As the MoS_2 loading increased, however, agglomeration and clustering behavior of the MoS_2 was visible, illustrating poor dispersion. Nonetheless, due to their conjugation with ethanethiol or nonanethiol, MoS_2 nanosheets could disperse homogeneously in chlorobutyl rubber at low concentrations. As shown in Figure 6, MoS_2-nonanethiol-butyl rubber had a more uniform appearance than MoS_2-ethanethiol-butyl rubber; at 5 phr MoS_2, in particular, the clustering for MoS_2-ethanethiol-butyl rubber was more pronounced than for MoS_2-nonanethiol-butyl rubber.

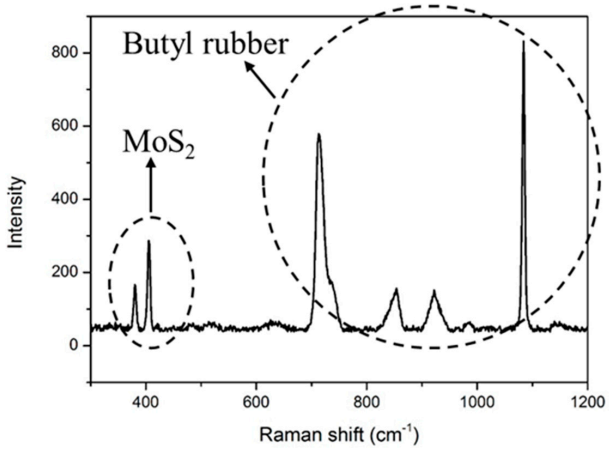

Figure 7. Typical Raman peaks for MoS_2-butyl nanocomposites.

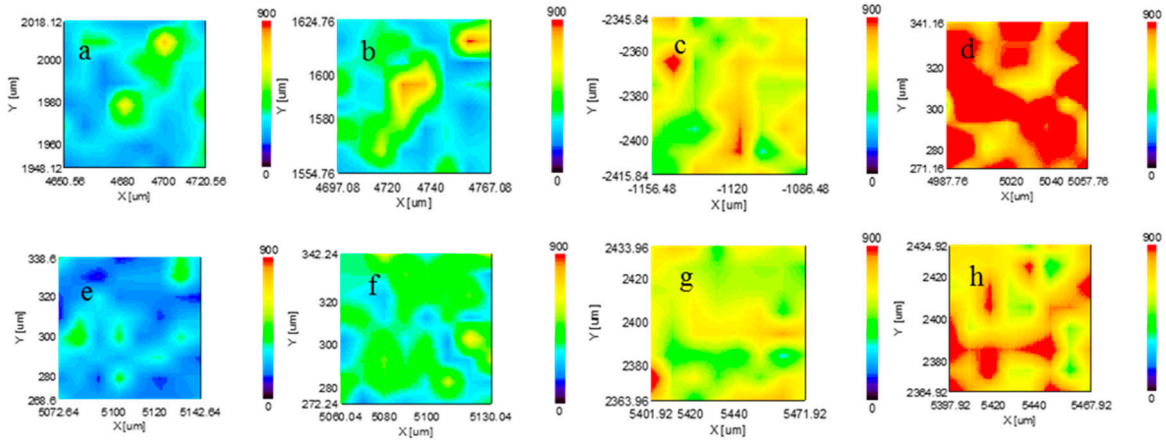

Figure 8. Raman mapping images for MoS_2-butyl rubber with different concentrations of MoS_2 with either ethanethiol or nonanethiol: (**a**) 0.5 phr, ethanethiol; (**b**) 1 phr, ethanethiol; (**c**) 3 phr, ethanethiol; (**d**) 5 phr, ethanethiol; (**e**) 0.5 phr, nonanethiol; (**f**) 1 phr, nonanethiol; (**g**) 3 phr, nonanethiol; and, (**h**) 5 phr, nonanethiol.

3.3. Tensile Properties of MoS_2-butyl Rubber Nanocomposites

The stress-strain curves (Figure 9) for neat chlorobutyl rubber and MoS_2-butyl rubber nanocomposites show that the tensile strength of the chlorobutyl rubber matrix increased upon MoS_2 nanosheet loading. Furthermore, the elongation at break of MoS_2-nonanethiol-butyl rubber was about 14.4% higher than that of MoS_2-ethanethiol-butyl rubber. The maximum increase in tensile strength for MoS_2-ethanethiol-butyl rubber was about 30.7% for a MoS_2 content of 3 phr. In MoS_2-nonanethiol-butyl rubber, likewise, the tensile strength was increased by about 34.8% for 1 phr MoS_2 as compared to that of the control sample. Therefore, the maximum increase in tensile strength was obtained for MoS_2-nonanethiol-butyl rubber instead of MoS_2-ethanethiol-butyl rubber. The significant increase

in tensile strength reached a peak at a loading of 3 phr for MoS_2-ethanethiol-butyl rubber and of 1 phr for MoS_2-nonanethiol-butyl rubber. At higher MoS_2 nanosheet contents, the tensile strength decreased again. The latter observations may be ascribed to the aggregation of MoS_2 nanosheets in the chlorobutyl rubber matrix, which is known to cause a decrease in tensile strength for rubber [26]. It is obvious from these results that MoS_2 nanosheets can significantly improve the strength of chlorobutyl rubber, possibly due to the high strength of MoS_2 nanosheets, better interactions between MoS_2 nanosheets and the polymer matrix, and/or a more uniform dispersion of MoS_2 nanosheets in the chlorobutyl rubber matrix due to abundant thiol groups on the MoS_2 nanosheet surfaces.

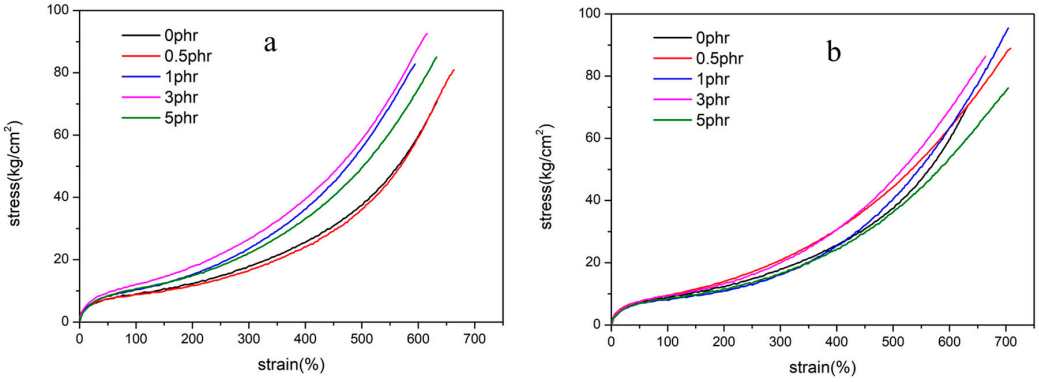

Figure 9. Stress-strain curves: (**a**) MoS_2-ethanethiol-butyl and (**b**) MoS_2-nonanethiol-butyl rubber.

3.4. Dynamic Mechanical Analysis of MoS_2-butyl Rubber Nanocomposites

For MoS_2-ethanethiol-butyl rubber, the storage modulus (Figure 10a) is a measure of its stiffness and the elastic of material that means the ability to recover pristine shape, and it a little increased for all the MoS_2-butyl rubber nanocomposites in rubbery region compared to pure chlorobutyl rubber but no significant increment in glassy region. In rubbery region, the nanocomposite containing 0.5 phr MoS_2 nanosheets exhibited the highest modulus value. MoS_2-nonanethiol-butyl rubber also showed an increase in the storage modulus (Figure 10b), with an increase in the content of MoS_2 nanosheets, except for 0.5 phr, and reached the highest modulus value for 3 phr. These results indicate that MoS_2 nanosheet incorporation into chlorobutyl rubber remarkably enhanced stiffness and had a significant reinforcing effect. This increase in storage modulus results from the intercalation of MoS_2 nanosheets in chlorobutyl rubber and strong interactions between the chlorobutyl rubber polymer chain and MoS_2 nanosheets. The mobility of the polymer chains in rubbery region was thus retarded by the MoS_2 nanosheets, resulting in the higher storage modulus.

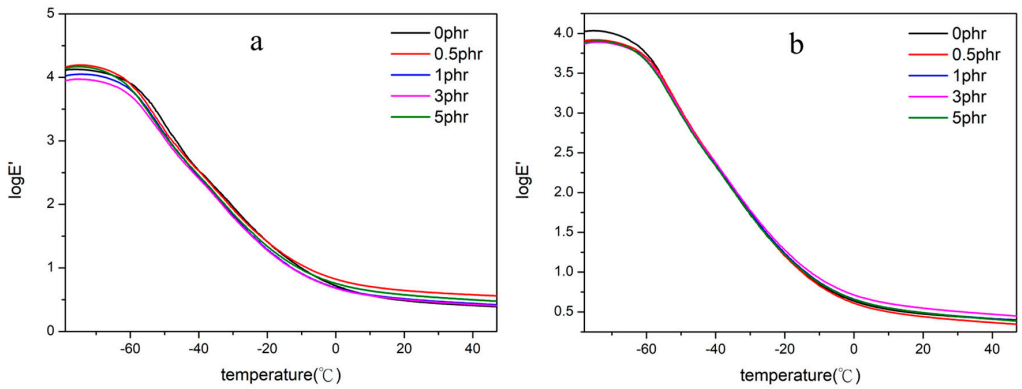

Figure 10. Storage modulus measurements: (**a**) MoS_2-ethanethiol-butyl and (**b**) MoS_2-nonanethiol-butyl rubber.

The tan(δ) values of MoS_2-ethanethiol-butyl rubber are shown in Figure 10a. For all of the samples of MoS_2-ethanethiol-butyl rubber, shifts to lower temperatures were observed when compared to the 0 phr sample. MoS_2 intercalated in chlorobutyl rubber may act as a lubricant, which leads to lowering of the glass transition temperature [27]. The tan(δ) values of MoS_2-nonanethiol-butyl rubber are shown in Figure 11b; similar shifts to lower temperatures can be seen, again indicating intercalation of MoS_2 nanosheets in the chlorobutyl rubber. The barrier effect of the nano-flakes restricting the motion of the polymer chains in the nanocomposites can be ascribed to the MoS_2 nanosheets.

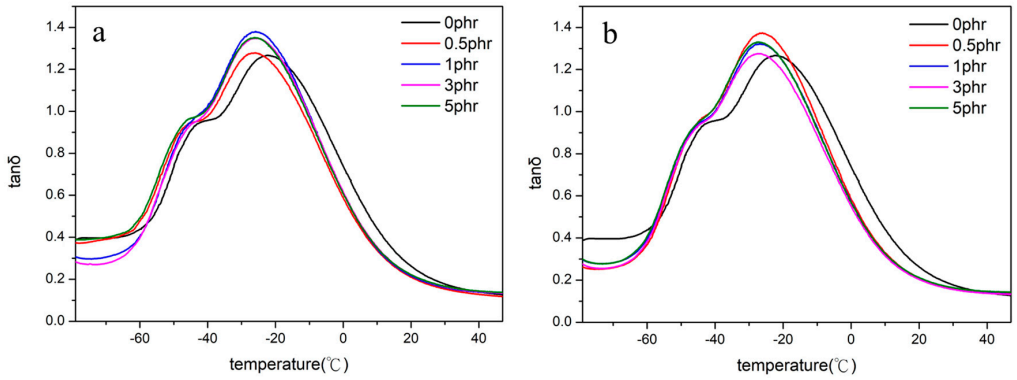

Figure 11. tan(*δ*) Measurements: (**a**) MoS_2-ethanethiol-butyl and (**b**) MoS_2-nonanethiol-butyl rubber.

3.5. Gas Barrier Properties of MoS_2-butyl Rubber Nanocomposites

The barrier properties of polymers can be significantly altered by including sufficient inorganic platelets to alter the path of gas molecules (Scheme 2) [4]. The oxygen transmission rate (OTR) (Table 1) of each MoS_2-butyl rubber nanocomposite was measured at 25 °C using the method outlined by ASTM D3985. When compared to that of pure chlorobutyl rubber, the OTR of MoS_2-ethanethiol-butyl rubber decreased dramatically to 42.3 cc/m^2-day at the MoS_2 nanosheet concentration of 0.5 phr. The OTR of MoS_2-nonanethiol-butyl rubber decreased to 47.2 cc/m^2-day at 0.5 phr, and thereafter decreased slowly at higher concentrations. The barrier performance for all MoS_2-butyl rubber nanocomposites could be improved markedly by the application of a small amount of organic-modified MoS_2. Moreover, there was little difference between the gas barriers of MoS_2-ethanethiol-butyl rubber and MoS_2-nonanethiol-butyl rubber, since the surface areas of MoS_2-ethanethiol and MoS_2-nonanethiol nanosheets were too small to retard the pathway of gas molecules. There are two reasons behind the enhancement of the gas barrier properties of the MoS_2-butyl rubber nanocomposites. First, MoS_2 nanosheets form tortuous pathways in chlorobutyl rubber, which retard the progress of gas molecules through the composite. Secondly, the diffusion coefficient of the gas molecules decreases because MoS_2 nanosheets strongly restrict the motion of the polymer chains [7].

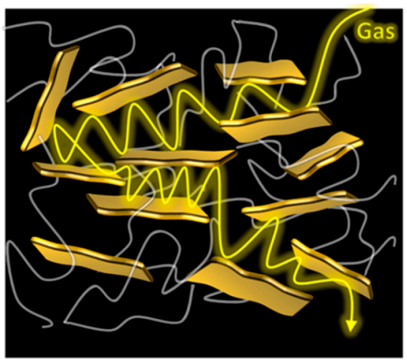

Scheme 2. Barrier to permeation imposed by nanoparticles embedded in a polymeric matrix.

Table 1. Oxygen transmission rates (OTRs) of MoS_2-butyl rubber nanocomposites.

	MoS_2-ethanethiol-butyl rubber (cc/m^2-day)	MoS_2-nonanethiol-butyl rubber (cc/m^2-day)
0 phr	90.9	90.9
0.5 phr	42.3	47.2
1 phr	48.2	46.8
3 phr	44.6	45.8
5 phr	43.7	46.5

4. Conclusions

In conclusion, we have demonstrated that MoS_2 nanosheets are an excellent filler material to enhance the tensile properties of chlorobutyl rubber. Ethanethiol and nonanethiol played an important role in modifying the surface of MoS_2 nanosheets. Using thiol modification of nanosheets helped to obtain MoS_2 monolayers with a thickness of ~0.8–1 nm, a key feature of MoS_2 nanosheets intercalated in chlorobutyl rubber. The obtained MoS_2 nanosheets were dispersed homogeneously in chlorobutyl rubber due to the thiol ligands modifying MoS_2 to enable greater affinity between MoS_2 and chlorobutyl rubber. Due to the high stiffness of the MoS_2 nanosheets, MoS_2 improved the mechanical properties of chlorobutyl rubber in tensile test, but not significantly in storage modulus. On the other hand, the gas barrier was improved dramatically, although similarly for MoS_2-ethanethiol- and MoS_2-nonanethiol-butyl rubber. These results offer new opportunities utilizing nanocomposites of polymers and MoS_2. Controlling the dimensions of MoS_2 nanosheets remains a challenge. Therefore, improved techniques are necessary to produce MoS_2 nanosheets of appropriate sizes, which can then achieve their full potential in polymer nanocomposites.

Acknowledgments: The authors would like to thank the Ministry of Science and Technology of the Republic of China (Taiwan) (grant number MOST 105-2622-E-011-009-CC2) for financially supporting this work.

Author Contributions: Chi-Yang Tsai, Shuian-Yin Lin and Hsieh-Chih Tsai conceived and designed the experiments; Chi-Yang Tsai performed the experiments; Chi-Yang Tsai and Hsieh-Chih Tsai analyzed the data; Chi-Yang Tsai wrote the paper.

Conflicts of Interest: The authors declare no conflict of interest.

References

1. Yoon, Y.; Ganapathi, K.; Salahuddin, S. How good can monolayer MoS_2 transistors be? *Nano Lett.* **2011**, *11*, 3768–3773. [CrossRef] [PubMed]
2. Anbazhagan, R.; Su, Y.-A.; Tsai, H.-C.; Jeng, R.-J. MoS_2-Gd chelate magnetic nanomaterials with core-shell structure used as contrast agents in in vivo magnetic resonance imaging. *ACS Appl. Mater. Interfaces* **2016**, *8*, 1827–1835. [CrossRef] [PubMed]
3. Feng, X.; Wen, P.; Cheng, Y.; Liu, L.; Tai, Q.; Hu, Y.; Liew, K.M. Defect-free MoS_2 nanosheets: Advanced nanofillers for polymer nanocomposites. *Compos. Part A* **2016**, *81*, 61–68. [CrossRef]
4. Paul, D.; Robeson, L.M. Polymer nanotechnology: Nanocomposites. *Polymer* **2008**, *49*, 3187–3204. [CrossRef]
5. Zachariah, A.K.; Geethamma, V.; Chandra, A.K.; Mohammed, P.; Thomas, S. Rheological behaviour of clay incorporated natural rubber and chlorobutyl rubber nanocomposites. *RSC Adv.* **2014**, *4*, 58047–58058. [CrossRef]
6. Liu, T.; Tjiu, W.C.; Tong, Y.; He, C.; Goh, S.S.; Chung, T.S. Morphology and fracture behavior of intercalated epoxy/clay nanocomposites. *J. Appl. Polym. Sci.* **2004**, *94*, 1236–1244. [CrossRef]
7. Liang, Y.; Cao, W.; Li, Z.; Wang, Y.; Wu, Y.; Zhang, L. A new strategy to improve the gas barrier property of isobutylene-isoprene rubber/clay nanocomposites. *Polym. Test.* **2008**, *27*, 270–276. [CrossRef]
8. Zheng, H.; Zhang, Y.; Peng, Z.; Zhang, Y. Influence of the clay modification and compatibilizer on the structure and mechanical properties of ethylene-propylene-diene rubber/montmorillonite composites. *J. Appl. Polym. Sci.* **2004**, *92*, 638–646. [CrossRef]
9. Galpaya, D.; Wang, M.; George, G.; Motta, N.; Waclawik, E.; Yan, C. Preparation of graphene oxide/epoxy nanocomposites with significantly improved mechanical properties. *J. Appl. Phys.* **2014**, *116*, 053518. [CrossRef]

10. Wu, J.; Huang, G.; Li, H.; Wu, S.; Liu, Y.; Zheng, J. Enhanced mechanical and gas barrier properties of rubber nanocomposites with surface functionalized graphene oxide at low content. *Polymer* **2013**, *54*, 1930–1937. [CrossRef]
11. Lian, H.; Li, S.; Liu, K.; Xu, L.; Wang, K.; Guo, W. Study on modified graphene/butyl rubber nanocomposites. I. Preparation and characterization. *Polym. Eng. Sci.* **2011**, *51*, 2254–2260. [CrossRef]
12. Fan, X.; Khosravi, F.; Rahneshin, V.; Shanmugam, M.; Loeian, M.; Jasinski, J.; Cohn, R.W.; Terentjev, E.; Panchapakesan, B. MoS_2 actuators: Reversible mechanical responses of MoS_2-polymer nanocomposites to photons. *Nanotechnology* **2015**, *26*, 261001. [CrossRef] [PubMed]
13. Patel, N.P.; Miller, A.C.; Spontak, R.J. Highly CO_2-permeable and selective polymer nanocomposite membranes. *Adv. Mater.* **2003**, *15*, 729–733. [CrossRef]
14. Ma, G.; Peng, H.; Mu, J.; Huang, H.; Zhou, X.; Lei, Z. In situ intercalative polymerization of pyrrole in graphene analogue of MoS_2 as advanced electrode material in supercapacitor. *J. Power Sources* **2013**, *229*, 72–78. [CrossRef]
15. Wang, T.; Zhu, R.; Zhuo, J.; Zhu, Z.; Shao, Y.; Li, M. Direct detection of DNA below ppb level based on thionin-functionalized layered MoS_2 electrochemical sensors. *Anal. Chem.* **2014**, *86*, 12064–12069. [CrossRef] [PubMed]
16. Chou, S.S.; De, M.; Kim, J.; Byun, S.; Dykstra, C.; Yu, J.; Huang, J.; Dravid, V.P. Ligand conjugation of chemically exfoliated MoS_2. *J. Am. Chem. Soc.* **2013**, *135*, 4584–4587. [CrossRef] [PubMed]
17. Zhou, W.; Zou, X.; Najmaei, S.; Liu, Z.; Shi, Y.; Kong, J.; Lou, J.; Ajayan, P.M.; Yakobson, B.I.; Idrobo, J.-C. Intrinsic structural defects in monolayer molybdenum disulfide. *Nano Lett.* **2013**, *13*, 2615–2622. [CrossRef] [PubMed]
18. Dungey, K.E.; Curtis, M.D.; Penner-Hahn, J.E. Structural characterization and thermal stability of MoS_2 intercalation compounds. *Chem. Mater.* **1998**, *10*, 2152–2161. [CrossRef]
19. Guan, G.; Zhang, S.; Liu, S.; Cai, Y.; Low, M.; Teng, C.P.; Phang, I.Y.; Cheng, Y.; Duei, K.L.; Srinivasan, B.M. Protein induces layer-by-layer exfoliation of transition metal dichalcogenides. *J. Am. Chem. Soc.* **2015**, *137*, 6152–6155. [CrossRef] [PubMed]
20. Bazylewski, P.; Divigalpitiya, R.; Fanchini, G. In situ raman spectroscopy distinguishes between reversible and irreversible thiol modifications in l-cysteine. *RSC Adv.* **2017**, *7*, 2964–2970. [CrossRef]
21. Marshall, C.P.; Marshall, A.O. The potential of raman spectroscopy for the analysis of diagenetically transformed carotenoids. *Philos. Trans. R. Soc. Lond. A Math. Phys. Eng. Sci.* **2010**, *368*, 3137–3144. [CrossRef] [PubMed]
22. Yin, W.; Yan, L.; Yu, J.; Tian, G.; Zhou, L.; Zheng, X.; Zhang, X.; Yong, Y.; Li, J.; Gu, Z. High-throughput synthesis of single-layer MoS_2 nanosheets as a near-infrared photothermal-triggered drug delivery for effective cancer therapy. *ACS Nano* **2014**, *8*, 6922–6933. [CrossRef] [PubMed]
23. Sim, D.M.; Kim, M.; Yim, S.; Choi, M.-J.; Choi, J.; Yoo, S.; Jung, Y.S. Controlled doping of vacancy-containing few-layer MoS_2 via highly stable thiol-based molecular chemisorption. *ACS Nano* **2015**, *9*, 12115–12123. [CrossRef] [PubMed]
24. Biswas, Y.; Dule, M.; Mandal, T.K. Poly(ionic liquid)-promoted solvent-borne efficient exfoliation of MoS_2/$MoSe_2$ nanosheets for dual-responsive dispersion and polymer nanocomposites. *J. Phys. Chem. C* **2017**, *121*, 4747–4759. [CrossRef]
25. Triantafillidis, C.S.; LeBaron, P.C.; Pinnavaia, T.J. Homostructured mixed inorganic-organic ion clays: A new approach to epoxy polymer-exfoliated clay nanocomposites with a reduced organic modifier content. *Chem. Mater.* **2002**, *14*, 4088–4095. [CrossRef]
26. Eksik, O.; Gao, J.; Shojaee, S.A.; Thomas, A.; Chow, P.; Bartolucci, S.F.; Lucca, D.A.; Koratkar, N. Epoxy nanocomposites with two-dimensional transition metal dichalcogenide additives. *ACS Nano* **2014**, *8*, 5282–5289. [CrossRef] [PubMed]
27. Choi, Y.S.; Choi, M.H.; Wang, K.H.; Kim, S.O.; Kim, Y.K.; Chung, I.J. Synthesis of exfoliated PMMA/Na-MMT nanocomposites via soap-free emulsion polymerization. *Macromolecules* **2001**, *34*, 8978–8985. [CrossRef]